FISEVIER

Contents lists available at ScienceDirect

Science of the Total Environment

journal homepage: www.elsevier.com/locate/scitotenv



Contribution of wastewater- versus non-wastewater-derived sources to haloacetonitriles formation potential in a wastewater-impacted river



Hamed Khorasani a, Jiale Xu a,b, Thuy Nguyen c, Zachary Kralles a, Paul Westerhoff Ning Dai a, Zhenduo Zhu a,*

- ^a Department of Civil, Structural and Environmental Engineering, University at Buffalo, Buffalo, NY 14260, USA
- ^b Department of Chemical and Environmental Engineering, University of Arizona, Tucson, AZ 85721, USA
- ^c School of Sustainable Engineering and the Built Environment, Arizona State University, Tempe, AZ 85287-3005, USA

HIGHLIGHTS

- A hydrodynamic and water quality model is developed for disinfection byproducts.
- Haloacetonitriles formation potential (HAN-FP) is measured for the Illinois River
- Both wastewater- and non-wastewaterderived sources of HAN-FP are considered
- HAN-FP concentration can be elevated under low flows due to wastewater contributions
- HAN-FP concentration can be elevated under high flows due to watershed runoff

GRAPHICAL ABSTRACT

Wastewater- and Non-wastewater-dervied Sources of Haloacetonitriles?



River Hydrodynamic and Water Quality Model

ARTICLE INFO

Article history: Received 18 March 2021 Received in revised form 15 May 2021 Accepted 5 June 2021 Available online 8 June 2021

Editor: Kevin V. Thomas

Keywords:
Disinfection by-product
Haloacetonitriles
Water reuse
Illinois River
Water quality modeling

ABSTRACT

Population growth and urbanization have led to the increasing presence of treated wastewater effluents in downstream drinking water sources. Drinking water sources influenced by organic matter from upstream wastewater treatment plant (WWTP) effluents are thought prone to the formation of haloacetonitriles (HANs), a group of nitrogenous disinfection by-products (DBPs) that can exhibit higher toxicity than currently regulated carbonaceous DBPs. We develop a framework for studying the HAN formation potential (HAN-FP) considering the WWTP and non-WWTP related sources of HAN precursors, and apply this framework to a representative WWTP-impacted river, the Illinois River, USA. A spatiotemporally-resolved river hydrodynamic and water quality model is developed using HEC-RAS to quantify the contribution of WWTP versus non-WWTP sources of HAN-FP precursors. Results show that non-WWTP sources of HAN-FP are considerable, accounting for up to 78% of HAN-FP concentration. Moreover, the contribution of the two sources varies due to streamflow discharge variability. During lower flows, the contribution of WWTPs drives the high concentration of HAN-FP and during higher flows, the contribution of non-WWTP sources becomes dominant. As a result, a high risk of HAN-FP may exist persistently (HAN-FP concentration is always larger than 9.7 µg/L in this study), not only during low flows but also during high flows due to both wastewater- and non-wastewater-derived HAN-FP sources.

© 2021 Elsevier B.V. All rights reserved.

1. Introduction

Access to clean water is vital for both drinking and hygiene purposes. Disinfection of public water supplies plays a pivotal role to inactivate the

^{*} Corresponding author. E-mail address: zhenduoz@buffalo.edu (Z. Zhu).

pathogens. Chlorine-based disinfectants are widely used, but reactions with natural organic matter (NOM) and inorganic compounds can form carcinogenic disinfection byproducts (DBPs) (Richardson and Postigo, 2015). Carbonaceous-DBPs (C-DBPs) include regulated trihalomethanes (THMs) and haloacetic acids (HAAs) (USEPA, 2010), but represent only a few of the more than 700 types of DBPs reported to occur in drinking waters (Thun et al., 2017). The relative importance of non-regulated DBPs remains debatable and research has been focusing on how different organic matter precursors influence concentrations of DBPs present in drinking water and their individual, or aggregate, toxicity (Diana et al., 2019). Most studies evaluate relative toxicity within drinking water treatment plants after different treatment processes are employed, but significantly less research is available regarding the dynamics and relative watershed sources of precursors responsible for forming non-regulated DBPs.

Many of the more toxic unregulated emerging DBPs appear to be nitrogenous DBPs (N-DBPs). Even though N-DBP concentrations are generally lower than C-DBPs, they can have a higher contribution to the cytotoxicity of drinking water than C-DBPs (Plewa et al., 2017; Shah and Mitch, 2012). After considering the concentration and toxicity of 11 groups of commonly detected DBPs (haloacetic acids, trihalomethanes, haloamides, haloaromatics, haloacetonitriles, haloacids, halodiacids, haloketones, halonitromethanes, haloaldehydes, and haloakenes), haloacetonitriles (HANs) emerge as having a higher risk than the other 10 DBP groups (Muellner et al., 2007; Plewa et al., 2017). Surveys have shown that the source waters impacted by wastewater and algal bloom are more prone to form N-DBPs (Dotson et al., 2009) as the formation of N-DBPs is related to the dissolved organic nitrogen (DON) concentration (Chen and Westerhoff, 2010). Water treatment plants have been shifting from use of free chlorine to chloramination to reduce the regulated DBPs, but chloramination tends to increase the formation of N-DBPs (Bond et al., 2011). With dynamic influences of wastewater discharges, shifts in disinfection practices increasing occurrence of algal blooms, and other watershed changes due to population growth or climate change, a need exists to better understand the dynamics of the more potentially toxic N-DBP precursors in freshwater resources serving as drinking water sources.

Potable water reuse is one of the responses to the increasing pressure on freshwater resources. While planned water reuse is an emerging endeavor that is integrated into water resources management (Darbandsari et al., 2020), unplanned water reuse (or de-facto reuse) in which source water is impacted by wastewater treatment plant (WWTP) effluents, is receiving attention in its human health impacts (NRC, 2012). Rice et al. (2013) used the drinking water treatment plant (DWTP) and WWTP databases across the US to provide an update to the 1980 nationwide EPA survey of de facto water reuse percentage (Swayne et al., 1980). Rice et al. (2013) showed that during the past three decades, de facto wastewater reuse has increased in more than two-thirds of the 25 most wastewater-impacted DWTPs; and that under low flow conditions, de facto reuse percentage ranges from 7% to 100%. Later, Rice and Westerhoff (2015) expanded the de facto reuse analysis to 1210 DWTPs across the US and found that in 32 DWTPs, during the low flow conditions, at least 50% of their intake water is treated wastewater effluents from the upstream.

By using a de facto reuse percentage or the dilution factor, researchers have tried to map the hotspots where the water quality is highly affected by the contaminants of emerging concern originated from WWTP effluents (Karakurt et al., 2019; Nguyen et al., 2018; Rice and Westerhoff, 2017; Siddiqui et al., 2020). Good and VanBriesen (2019) studied the contribution of wastewater effluent of coal-fired power plants on an important in-organic precursor (i.e., bromide ion) that becomes oxidized by chlorine and incorporated into DBPs. They used the median flow of the rivers and identified locations that may be at risk of increased higher brominated DBP. However, this approach does not identify background watershed patterns or the locations prone to increased DBP formation potential (DBP-FP) as a result of non-

wastewater sources. Kolb et al. (2020) utilized a simple regression model that predicts the total THM concentrations based on bromide and UV₂₅₄ to determine the impact of elevated bromide concentration as a result of coal power plant effluent in the Monongahela River basin. Using the average UV₂₅₄, they assessed the impact of flow discharge variability on bromide concentration and consequently on the THM concentration. Weisman et al. (2019) studied the de facto reuse percentage and the formation of two regulated DBPs (THMs and HAAs) in the Shenandoah River basin and found that there is a correlation between the DBP formation and increased de facto reuse percentage, especially when exceeding an annual de facto reuse level of 1%. However, to the authors' best knowledge, no study has focused on HANs to understand the contribution of wastewater- and nonwastewater-derived HAN precursors in a large river basin.

HAN-FP of water resources can increase as a result of the presence of wastewater effluent discharges (Iqbal et al., 2020; Roccaro et al., 2014). The concentration of HAN-FP in wastewater effluents depends on many factors and some reported values across the world are 6.1-38.8 µg/L in Australia (Doederer et al., 2014), 16.5 µg/L in Greece (Kozari et al., 2020), and 17-47 μg/L in Thailand (Phatthalung and Musikavong, 2019). The HAN-FP can also originate from non-wastewater sources (Chow et al., 2011; Zhang and Liang, 2019) but the contribution of the different sources has not been quantitatively assessed in the literature. In this study, we aim to develop a framework for modeling dynamics of HAN-FP in rivers, which considers both wastewater- and nonwastewater-derived sources using as the case study a highly wastewater impacted watershed (i.e., Illinois River basin). A spatially- and temporally-resolved water quality model is developed in Hydrologic Engineering Center River Analysis System (HEC-RAS) software to incorporate the information of WWTPs in the basin. Using the HAN-FP and water quality parameters of 10 samples from four stations (the urban headwater, two tributaries, and one downstream station for validation) for 4 months (from September to December 2019), the non-wastewater HAN-FP sources are estimated as a function of flow discharge and incorporated into the model. The contribution of wastewater- and nonwastewater-derived HAN-FP is analyzed for different flow conditions.

2. Materials and methods

A flowchart of the framework proposed for this study is presented in Fig. 1. The proposed framework is designed in three steps. In the first step the collection of data and inputs and in the second step the development of the models are shown, respectively. The third step is about the applications of the developed model that are mostly explained in Results section.

2.1. Study area and sampling locations

The Illinois River, a major tributary of the Mississippi River, is selected as the study area. With a length of 465 km, the Illinois River's headwater is located in the Chicago Metropolitan Area and it joins the Mississippi River near Grafton, Illinois (see Fig. 2). The Illinois River was originally isolated from the Great Lakes basin, but due to the construction of nearly level channels and changing the flow direction in the Chicago River, they have been connected for over a century (Bellrose et al., 1966). The City of Chicago (population about 2.7 million), as part of the Chicago Metropolitan Area (population about 9.5 million), is located upstream of the Illinois River. Lake Michigan is the source of water for the Chicago Metropolitan Area.

With the assistance of the U.S. Geological Survey, water samples were collected from four sampling locations and shipped on ice to University at Buffalo for analysis (details in Section 2.3). The sampling locations were selected from the list of the current stations so that the measurements of discharge on the day of sampling are available. The land use and land cover of the watersheds upstream of the sampling locations, as explained in the following and shown in Fig. 2, were the

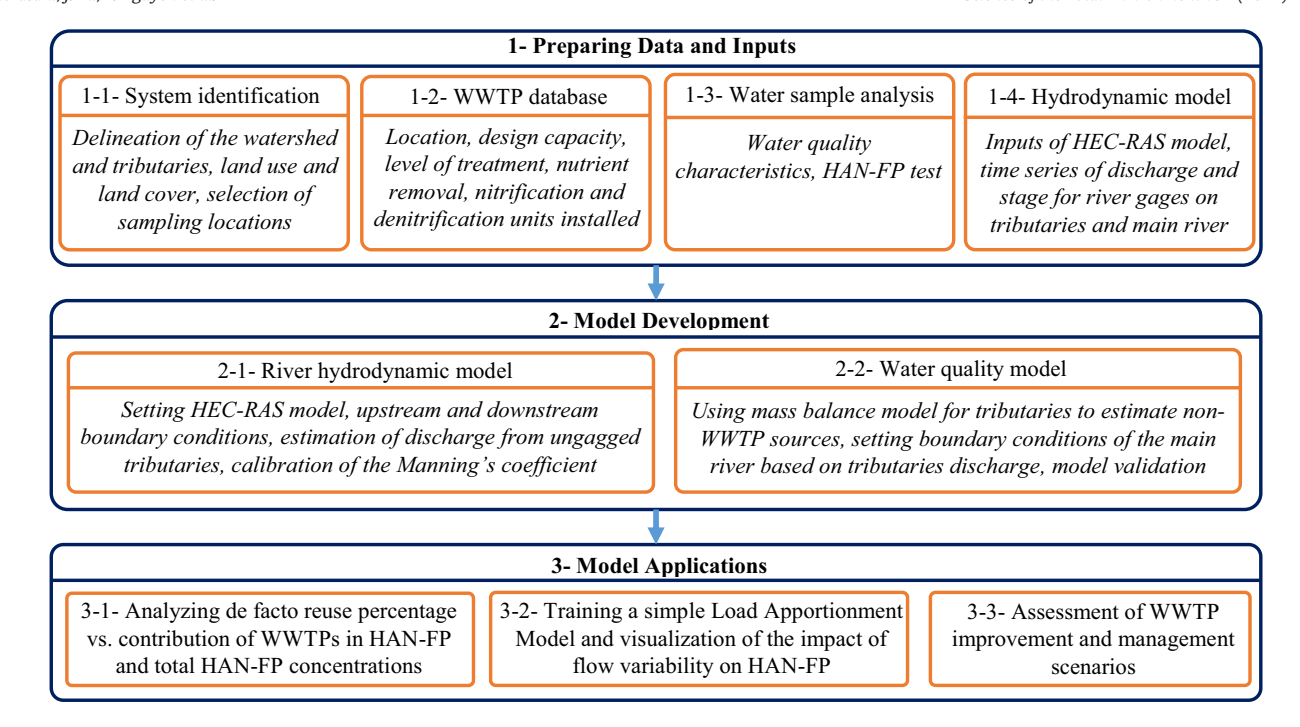


Fig. 1. The flowchart of the framework developed in this study.

most important criteria for their selection. The Des Plaines River at Route 53 at Joliet, IL is the most upstream station among the four stations and 73% of its watershed is developed and urbanized land use. The Kankakee River near Wilmington and the Fox River at Ottawa stations are in two major tributaries and their land use is mainly crop, pasture, and forest, which are similar to the land use and land cover of other tributaries. The Illinois River at Henry is the most downstream sampling station; although its watershed includes the upstream Chicago urban regions, it has mainly agricultural and natural land use: only 21% of urban developed land and 79% non-developed land cover due to the high percentage of agricultural and natural land use in other tributaries. Overall, 71% of land use and land cover in the Illinois River watershed is cropland and pasture, 12% is forest, and 14% is urban developed land use (Fig. 2, See Table S1 for more details).

Each site was sampled 2–3 times over 4 months from September to December in 2019. Overall, 10 samples were gathered and Table S2 shows the sampling dates and the water quality parameters of each sample.

2.2. Information on location and characteristics of WWTPs

The EPA Clean Watersheds Needs Survey (CWNS) 2012, released in May 2016, provided the WWTP facility information including design capacity, National Pollutant Discharge Permit (NPDES) number, level of treatment (primary, secondary, or advanced treatment), and locations of wastewater outfalls to surface water (USEPA, 2016). In this study, there are 299 WWTPs with a total design capacity of 2743 million gallons per day (MGD), approximately equal to 120 m³/s, that discharge into surface waters in the Illinois River basin. Approximately 55% of the 299 WWTPs have a relatively small treatment capacity below 1 MGD (See Table S3 for flow range).

The NPDES permit regulates the minimum removal standards of municipal effluents before discharging into surface waters which include a five-day biochemical oxygen demand (BOD₅) concentration (30-day average), total suspended solids (TSS) removal, pH, and level of treatment. The level of treatment of effluents is considered to be providing when the effluents meet the required standards of BOD₅ with greater than 45 mg/L (primary treatment), greater than 30 mg/L but less than or equal to 45 mg/L (advanced primary treatment), less than or equal to

30 mg/L (secondary treatment), greater than 10 mg/L but less than or equal to 20 mg/L (advanced treatment I), or less than 10 mg/L (advanced treatment II) (USEPA, 2016). Any level of treatment with nutrient removal indicates a higher quality of treated effluents in the removal of nitrogen and phosphorus. Approximately 40% of the 299 WWTPs (n = 119) employ secondary treatment (the minimum level of treatment required by NPDES before discharging into surface waters). Only one-fourth of the WWTPs (n = 75) are equipped with unit processes to remove nutrients from about 85% of the total design capacity (or 2326 MGD) of WWTP effluents in the Illinois River basin (Table S4). Krasner et al. (2009) conducted a nationwide survey to assess the impact of wastewater treatment processes, specifically whether nitrification is practiced, on the DBP formation potential of the effluents: the median, 25th percentile, and 75th percentile of the HAN-FP for nitrified effluents is 13.0 µg/L, 12.0 µg/L, and 19.0 µg/L, respectively; the corresponding values for non-nitrified effluents are 28.5 $\mu g/L$, 18.3 $\mu g/L$, and 32.8 $\mu g/L$, respectively (See Table S5). We used these values to estimate the HAN-FP loading from WWTP effluents in water quality modeling.

2.3. Ancillary water quality analysis

Aliquots of the unfiltered sample were used to measure turbidity (NTU) using a Hach 2100Q portable turbidimeter (Hach Company, USA). Other water quality parameters and DBP formation potential were measured after filtration. Upon arrival, samples were filtered immediately through pre-combusted 0.7 µm glass fiber filters, stored at 4 °C, and analyzed within one week. The concentration of ammonia (NH₃, mgN/L) nitrogen was measured by Hach salicylate colorimetric method (Hach Company, 2015). The concentrations of nitrate (NO₃, mgN/L), nitrite (NO₂⁻, mgN/L), chloride (Cl⁻, mg/L), and bromide (Br⁻, mg/L) were measured by an ICS - 1000 ion chromatography system (Dionex, Sunnyvale, CA). Dissolved organic carbon (DOC, mgC/L) and dissolved total nitrogen (TN, mgN/L) were analyzed by a TOC-L/TN analyzer (Shimadzu Corp., Kyoto, Japan). The concentration of dissolved organic nitrogen (DON, mgN/L) was obtained by subtracting the sum of ammonia, nitrite, and nitrate concentrations from the total nitrogen concentration. UV absorbance at 254 nm (UVA₂₅₄, cm⁻¹) was measured using a Cary 60 UV-Vis Spectrophotometer (Agilent Technologies, CA, USA). Sample pH was measured using a SevenCompact pH/Ion meter (Mettler Toledo,

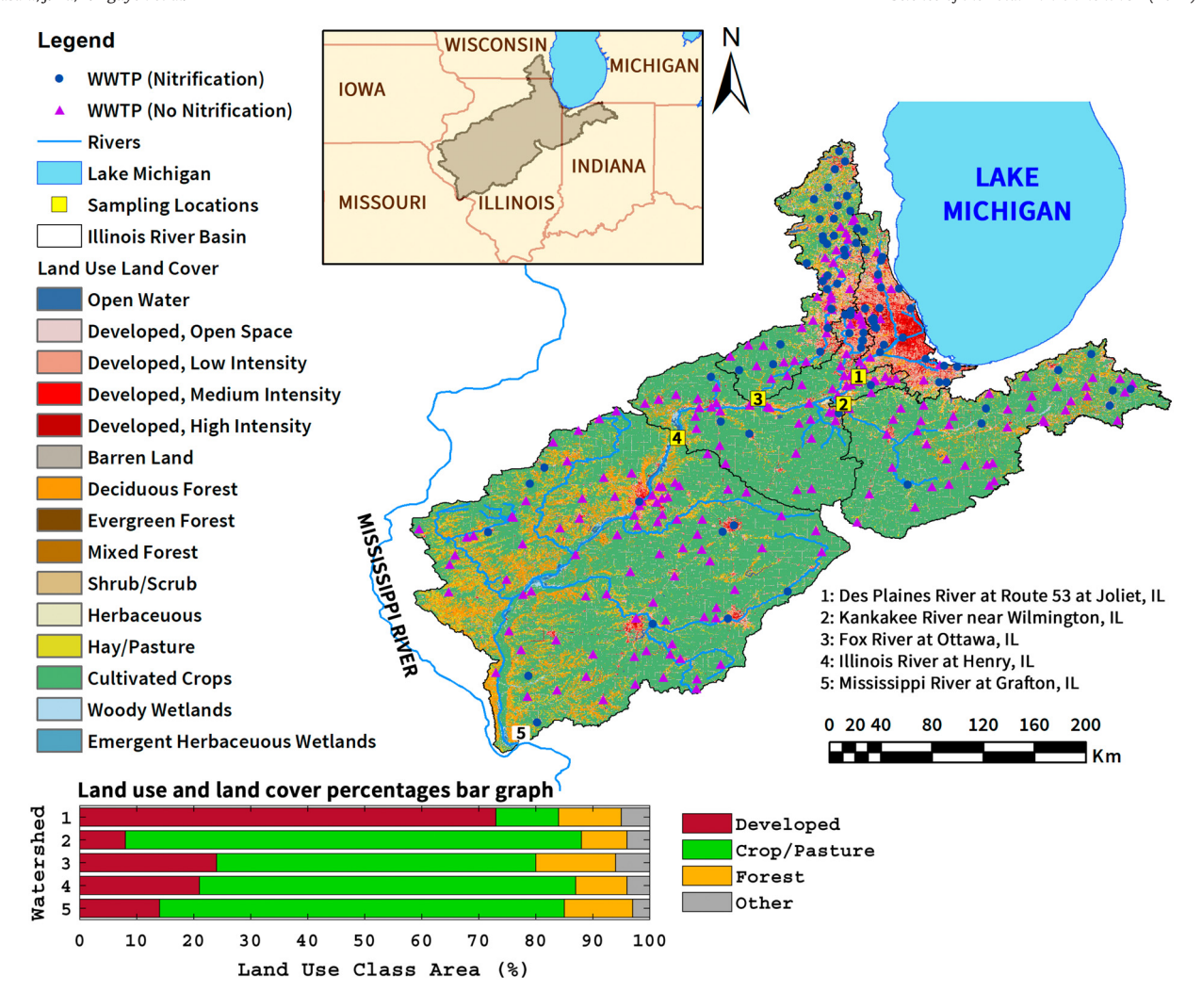


Fig. 2. The Illinois River basin and its land use and land cover percentage, the locations of the WWTPs, and the sampling locations for water quality measurements. The watershed IDs in the land use percentage graph are corresponding to the sampling location IDs as indicated on the map. The Mississippi River at Grafton, IL station is the outlet of the whole Illinois River basin.

Columbus, OH). The detection limits for the aforementioned water quality parameters are as follows: turbidity (0.05 NTU), NH $_3$ (0.03 mgN/L), NO $_3^-$ (0.02 mgN/L), NO $_2^-$ (0.02 mgN/L), Cl $^-$ (0.02 mg/L), Br $^-$ (0.03 mg/L), TN (0.1 mgN/L), and DOC (0.1 mgC/L).

2.4. HAN-FP measurement

The DBP-FP test followed a previously published protocol (Chen and Westerhoff, 2010; Krasner et al., 2009). Samples were buffered at pH 7.2 with 10 mM phosphate buffer. The chlorine dose applied to each sample was determined based on the DOC and NH3-N levels in the sample in order to ensure the presence of chlorine residual after 24 h: NaOCl (mgCl₂/L) = $3 \times$ DOC (mgC/L) + $8 \times$ NH3 (mgN/L) + 10. After chlorine addition, samples were kept in the dark at room temperature for 24 h, after which residual chlorine was quenched by 0.5 g/L of sodium thiosulfate. Samples before and after the FP tests were analyzed for four HANs (dichloroacetonitrile (DCAN), bromochloroacetonitrile (BCAN), dibromoacetonitrile (DBAN), and trichloroacetonitrile (TCAN)). The DBP-FP was calculated as follows:

$$FP = C_{After} - C_{Before} \tag{1}$$

where C_{after} and C_{before} are the DBP concentrations (µg/L) measured after and before the FP test, respectively.

Samples (30 mL) were spiked with the internal standard 1,2-dibromopropane (10 µg/L), mixed with 10 g sodium sulfate, and then

solvent-extracted using 2 mL *tert*-butyl methyl ether (MtBE). The extracts were analyzed by a gas chromatography-electron capture detector (GC-ECD, Agilent 7890B—63Ni ECD) with an HP-5 column using a previously developed method (Xu et al., 2020, 2019). Briefly, 3 μ L of MtBE extract was injected in splitless mode at 150 °C; column temperature was held at 26 °C for 9 min, and then raised to 60 °C at 25 °C/min and held for 1 min, and then raised to 100 °C at 20 °C/min and held for 1 min, and then raised to 250 °C at 70 °C/min and held for 1 min; ECD temperature was 290 °C, and the makeup gas was a mixture of methane and argon with a flow rate of 18.8 mL/min. The minimum detection limit is 0.1 μ g/L for HANs.

$2.5.\,A\,spatially-\,and\,\,temporally-resolved\,\,water\,\,quality\,\,model$

In this section, the components of the river hydrodynamic and water quality modeling are described. Two main scenarios are considered for simulating HAN-FP in the river: (i) considering only WWTPs as the sources of HAN-FP and (ii) incorporating the estimated non-WWTP sources in addition to WWTPs into the modeling. The development of this water quality model enables us to estimate the contribution of the WWTPs in the HAN-FP at any time and location by dividing the concentration of the HAN-FP in the first scenario by that in the second scenario. We also investigate the relationship between the de facto water reuse percentages which is defined as total upstream WWTP discharge by the streamflow discharge at any location.

2.5.1. River hydrodynamic modeling

The U.S. Army Corps of Engineers (USACE) Hydrologic Engineering Center River Analysis System (HEC-RAS) software (USACE, 2016) was used for developing a one-dimensional unsteady river hydrodynamic model. Streamflow dynamics are simulated based on the Illinois River hydrodynamic model previously developed by Zhu et al. (2018). There are 48 tributaries considered in the model in addition to the urban headwater upstream of the Des Plaines River, including the Chicago Area Waterway System, which is incorporated as the upstream boundary condition. The upstream boundary condition was obtained from the USGS gauge at the Des Plaines River at Route 53 at Joliet (USGS 05537980), while the downstream boundary condition was obtained from the USGS gauge at the Mississippi River at Grafton, IL (USGS 05587450). Fifteen tributaries that correspond to 73% of the Illinois River basin are monitored by USGS gauges, while the other ungagged tributaries' flow discharges are calculated by the drainage area ratio method as explained by Zhu et al. (2018). The model was modified by implementing new boundary conditions for all tributaries and calibrated for the simulation period of September-December 2019 using the USGS gaging stations along the river. Using the output time interval of 15 min, the Manning's roughness coefficient was calibrated with the automated calibration option in HEC-RAS for each river segment that is the river channel between two USGS gauges.

2.5.2. Water quality modeling

The water quality module in HEC-RAS utilizes an explicit numerical method to solve the 1D advection-dispersion equation with first-order growth/decay as follows (USACE, 2016):

$$\frac{\partial C}{\partial t} + U \frac{\partial C}{\partial x} = D \frac{\partial^2 C}{\partial x^2} + KC \tag{2}$$

where C is the HAN-FP concentration (μ g/L), t is time (s), U (m/s) is the average advective velocity of the river flow in x direction (along the river), D is the dispersion coefficient (m^2/s) that is intrinsically calculated in the model based on characteristics of the flow and geometric quantities of the channel, and *K* is the growth/decay rate constant representing the transformation of the HAN-FP (input in the model in day⁻¹). Because typical drinking water treatment processes are effective in removing particulate DBP precursors, the dissolved fraction is the primary focus of this study. Accordingly, the settling process was not considered for HAN formation potential. However, it is worth mentioning that the dissolved HAN precursors can interact with colloidal and particulate matter that is subjected to settling. Biogeochemical processes of the precursor of DBPs are generally highly dependent on the sources the organic matter (Lee and Hur, 2014) and they sometimes can have opposite outcomes. For example, the biodegradation within the timescale relevant to the hydraulic residence time of the modeling domain (a couple of weeks) had no significant change in the HAN-FP of the source water from forests (Chow et al., 2013); while the microbial biodegradation before disinfection is considered as an effective strategy to reduce the HAN-FP in drinking water treatment plants (Zhang et al., 2019). As for the photo-transformation, photolysis is shown to not affect the HAN-FP of the source water from the forest (Tsai et al., 2015) or even it can significantly increase HAN-FP in source water (Chow et al., 2013), while the solar radiation can significantly decrease the HAN-FP of reclaimed wastewater (Qian-Yuan et al., 2016). Different types of N-DBPs also have divergent responses to solar radiation. For example, while DCAN-FP is significantly reduced in wastewater effluent and a mixture of treated wastewater and surface water (Wu et al., 2018; Xu et al., 2020), the trichloronitromethane (TCNM) FP is actually increased in the mixture of treated wastewater and surface water (Wu et al., 2018). As a result of this divergent evidence, we decided to assume that the total HAN-FP does not decay or grow and neglected the transformation of different precursors of HANs to each other.

The boundary conditions, i.e. the HAN-FP concentrations in the tributaries, are a crucial input for the water quality model. The boundary conditions were set as two scenarios to evaluate the relative importance of WWTP and non-WWTP sources. In the first scenario, only WWTP sources of HAN-FP were considered, while in the second scenario, the non-WWTP sources were also estimated and incorporated into the model. The non-WWTP sources of HAN-FP are the surface water runoff or leachate from different land covers including irrigation runoff from agricultural lands, surface runoff from forests and grasslands that transports the natural organic matter and the precursors of HAN-FP into the waterways (Chow et al., 2011; Eckard et al., 2020). The next section explains how the WWTP and non-WWTP sources were estimated.

2.5.3. Estimation of the wastewater and non-wastewater sources of HAN-

Since the individual tributary watersheds are considerably smaller than the mainstem of the Illinois River, we assume that modeling HAN-FP within the tributaries can be done using a simple mass balance equation. The mass balance approach simply assumes that the summation of WWTP and non-WWTP loadings of HAN-FP divided by the streamflow discharge at the tributary outlet is equal to the HAN-FP concentration at the tributary outlet. This mass balance approach is used to estimate the non-WWTP loadings of HAN-FP in the tributaries, assuming that we know the estimation of HAN-FP loading from WWTPs (Section 2.2) as well as the total loadings based on samplings. About 94% of the WWTPs in the Illinois River basin (281 out of 299) are located within one of the 48 tributaries or the urban headwater upstream of the Des Plaines River. Eighteen other WWTPs are located very close to the main Illinois River while not within any distinguishable tributaries; therefore, their effluent is assumed to be directly released into the Illinois River in the closest water quality computational cell.

After knowing the WWTP sources, the following mass balance equation was used to calculate the non-WWTP sources. The load (L) of HANFP in a specific tributary is the summation of loads of FP from WWTP and non-WWTP sources as follows:

$$L_{Trib} = L_{WWTPs} + L_{non-WWTPs}$$
 (3)

where L_{Trib} is the total load of the HAN-FP (g/s) at the outlet where the tributary joins the mainstem Illinois River; L_{WWTPs} and $L_{non-WWTPs}$ are the loads from WWTP and non-WWTP sources within the tributary, respectively. Given that loading is the multiplication of discharge (Q, m^3 /s) and HAN-FP concentration (C, μ g/L), Eq. (3) can be rewritten as follows:

$$\label{eq:trib} \begin{aligned} Q_{\textit{Trib}} \cdot C_{\textit{Trib}} &= \sum \left(Q_{\textit{WWTP}_i} \cdot C_{\textit{WWTP}_i} \right) + Q_{\textit{non-WWTP}} \cdot C_{\textit{non-WWTP}} \end{aligned} \tag{4}$$

where the total discharge (Q_{Trib}) and the HAN-FP concentration (C_{Trib}) of the tributary can be measured where the tributary joins the Illinois River; the discharge (Q_{WWTP_i}) and the HAN-FP concentration (C_{WWTP_i}) of ith WWTP that are known as discussed in Section 2.2; and the non-WWTP streamflow $(Q_{non-WWTP})$ is the remaining flow in the tributary that is not originated from WWTPs $(Q_{Trib}-Q_{WWTP_s})$. Thus Eq. (4) can be rearranged to the following to calculate the HAN-FP weighted-average concentration of non-WWTP sources $(C_{non-WWTP})$:

$$C_{non-WWTP} = \frac{Q_{Trib} \cdot C_{Trib} - Q_{WWTPs} \cdot C_{WWTPs}}{Q_{non-WWTP}}$$
(5)

The non-WWTP sources are most likely related to the non-point sources. Since an increase in river streamflow is often a result of increased surface runoff that can alter the delivery of non-point sources to the river (Borisover et al., 2011; Li et al., 2019; Yin et al., 2021), we tried to correlate $C_{non-WWTP}$ with $Q_{non-WWTP}$, i.e. $C_{non-WWTP} = f(Q_{non-WWTP})$. Hence, it is assumed that $C_{non-WWTP}$ is a function of the river flow discharge, and we used regression analysis to estimate this function.

Table 1Model calibration results of the hydrodynamic model at nine USGS stations.

Gauge number	River Km	Station name (Illinois River at)	Station ID number	Data	NSE	RSR	PBIAS
1	60.43	Seneca, IL	USGS 05543010	Stage	0.97	0.17	0
2	69.54	Marseilles, IL	USGS 05543500	Stage	0.97	0.17	0
2	69.54	Marseilles, IL	USGS 05543500	Flow	0.97	0.17	1
3	150.81	Henry, IL	USGS 05558300	Stage	0.91	0.30	0
3	150.81	Henry, IL	USGS 05558300	Flow	0.97	0.18	1
4	232.10	Kingston Mines, IL	USGS 05568500	Stage	0.94	0.24	0
4	232.10	Kingston Mines, IL	USGS 05568500	Flow	0.84	0.41	-1
5	246.18	Copperas Creek, IL	USGS 05568615	Stage	0.94	0.25	0
6	351.41	Meredosia, IL	USGS 05585500	Stage	0.92	0.28	0
7	367.52	Valley City, IL	USGS 05586100	Stage	0.89	0.34	0
7	367.52	Valley City, IL	USGS 05586100	Flow	0.56	0.66	11
8	376.05	Florence, IL	USGS 05586300	Stage	0.94	0.25	0
9	431.41	Hardin, IL	USGS 05587060	Stage	0.98	0.13	0

2.5.4. Training a simple model considering flow variability

The riverine pollutants that have both point and non-point sources, e.g. nutrients, can be modeled in watersheds as a function of discharge. This empirical modeling approach uses formulae in a way that allows not only the simulation of the concentration of the pollutant but also the specification of the contribution of different sources. Load Apportionment Model (LAM) is one of the well-known models developed by Bowes et al. (2008), which is composed of two power functions for modeling the concentration of a substance as a function of streamflow discharge. The first function represents the concentration due to point sources (i.e. WWTP sources in this study) and the second power function represents the concentration due to non-point sources (i.e. non-WWTP sources). The formulation of the LAM models is as follows (Bowes et al., 2008):

$$C_{IR} = aQ_{IR}^b + cQ_{IR}^d \tag{6}$$

where C_{IR} is the concentration of HAN-FP (µg/L) and Q is the streamflow of the Illinois River (m³/s). The constraints in the training of this equation are b < 0 (since the points sources are supposed to dilute as the streamflow increases) and d > 0 (as the streamflow increases, the contribution of non-point sources also increases). This model was applied to train a simple management model so that decisions can be made quickly without running the spatially- and temporally-resolved water quality model.

3. Results and discussion

3.1. River hydrodynamic modeling

The unsteady and spatially-varied hydrodynamic model of the Illinois River was calibrated using the stage data of 9 USGS gauges as presented in Table 1. To assess the performance of the model, Nash-Sutcliffe Efficiency (NSE), the ratio of root-mean-squared-error to the standard deviation of measured data (RSR), and percent bias (PBIAS), as well as graphical analysis, are employed (See Text S1 for details). Moriasi et al. (2007) reviewed reported ranges of performance statistics for watershed hydrologic modeling and established a comprehensive guideline for evaluating simulation results regarding streamflow, sediment, and nutrients in the monthly time step. Based on this monthly guideline, an NSE > 0.75, RSR ≤ 0.50 , and PBIAS $\le \pm 10$ would indicate a "very good" performance of the streamflow modeling.

Considering that the calculated values in Table 1 are based on a time step of 15 min which is much smaller than a monthly time step, the performance of all gauges falls in the "very good" performance rating except for the streamflow at the station USGS 05586100 Illinois River at Valley City, IL. With a PBIAS of 11, the streamflow simulation in this station falls in the "good" performance rating category while for the NSE and RSR metrics, the station falls only in the "satisfactory" performance rating when using the strict metrics of Moriasi et al. (2007).

For daily and intra-daily time steps, the monthly time step guidelines can be relaxed. For example, Kalin et al. (2010) have adapted similar guidelines to daily time step modeling. The NSE performance criteria of the Illinois River at Valley City, IL falls in the "good" performance rating $(0.50 \le NSE < 0.70)$ using the daily time step guidelines provided by Kalin et al. (2010).

The simulated and observed stages in two stations (USGS 05558300 and 05586300), as well as the simulated and observed streamflow discharges at two stations (USGS 05543500 and 05568500), are illustrated in Fig. 3 (See Fig. S1 for the location of the stations on map). The simulation starts from September 1, 2019, with a relatively low flow followed by two high flow events in October and November, and then the system experiences less flow variability towards the end of December. Flow duration curves that express the percent of the time that streamflow discharge exceeds a particular discharge are used for the analysis of high and low flows. Using the flow duration curve analysis for the Des Plaines River at Route 53 at Joliet (River km = 1.4), Illinois River at Henry (River km = 150.8), and Illinois River at Valley City (River km = 367.5), two days are chosen to represent relatively high and low flows. With the flow duration of 3.6%, 1.0%, and 26.5%, respectively at the three chosen gauges, October 1, 2019, is chosen as the representative of the high flow situation. This means that the flow discharge is so high that for example, only 1.0% of the time the Henry station has recorded higher flows. December 20, 2019, is chosen as the representative of the low flow with flow duration discharge of 77.0%, 59.6%, and 51.3% at the aforementioned gauges, respectively.

3.2. Water quality modeling and estimation of non-wastewater sources of HAN-FP

Estimates of non-WWTP sources were conducted using linear regression analysis of the non-WWTP HAN-FP and the non-WWTP streamflow discharge estimated in the three tributaries (one urban headwater upstream of Des Plaines River, and two major nonurbanized tributaries upstream of Fox River and Kankakee River). The initial analysis showed that the behavior of the Fox River and Kankakee River watersheds are similar to each other, but very different from the Des Plaines River watershed where urban/developed land cover dominates the land area (See Fig. 2 and Table S1). Regression analysis results for the estimation of the non-WWTP sources of HAN-FP are shown in Fig. 4. Based on data in Fig. 4a, a linear relationship was established between the non-WWTP streamflow and non-WWTP HAN-FP in the two non-urban tributaries. However, Fig. 4b shows no meaningful relationship within the Des Plaines River urban headwater, partially because there are only three observations available for this station and the HAN-FP data are highly variable. The regression analysis resulted in Eq. (7) for estimation of the non-WWTP sources of HAN-FP in the non-urbanized tributaries of the Illinois River as a function of their corresponding non-WWTP streamflow discharge.

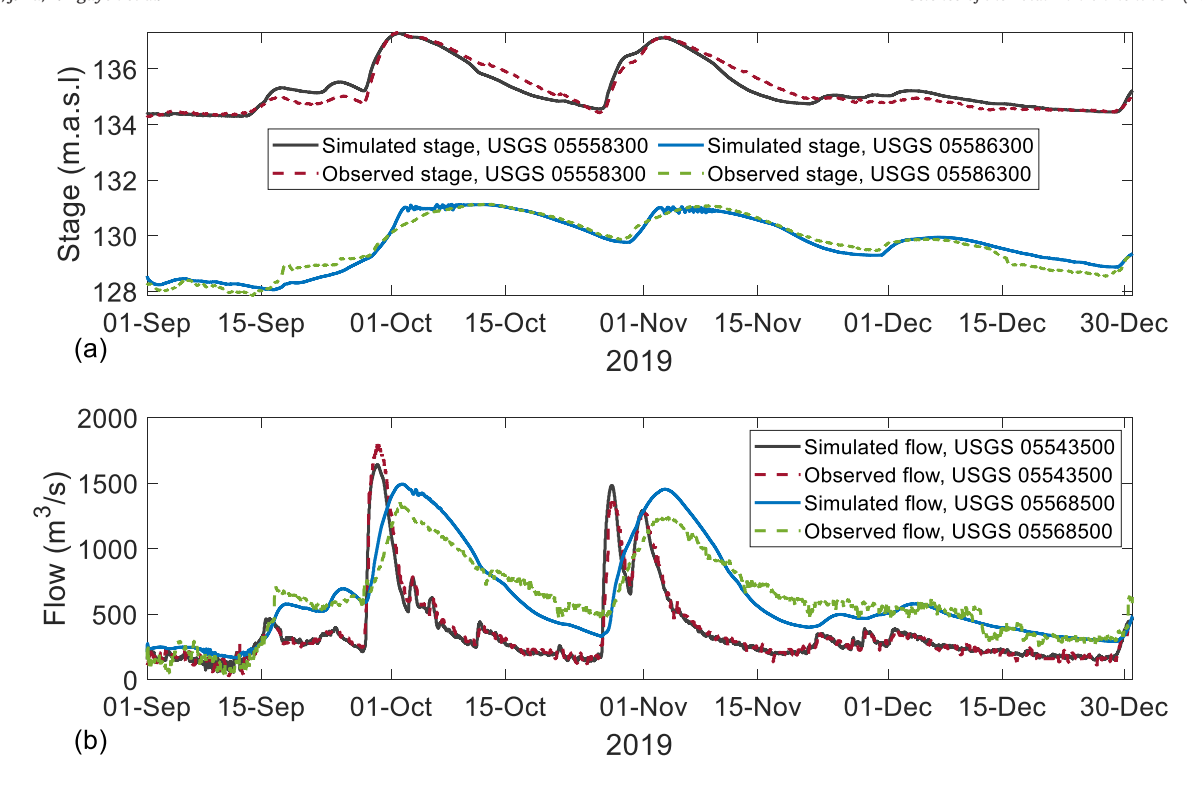


Fig. 3. Comparison of the measured and simulated results for (a) river stage (meter above sea level, m.a.s.l) at USGS gaging stations (05558300 and 05586300) and (b) streamflow discharge (m³/s) at USGS gaging stations (05543500 and 05568500) on the Illinois River during Sep. 01–Dec. 31, 2019.

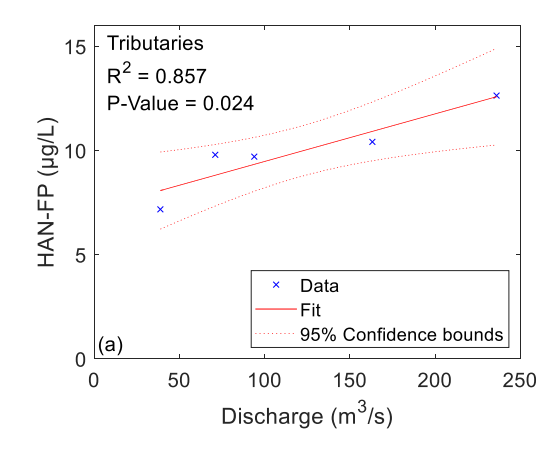
While for the urban headwater upstream of the Des Plaines River, the average value of the estimated non-WWTP HAN-FP which is equal to $10.68 \ \mu g/L$ is used.

$$C_{non-WWTP} = \left\{ egin{array}{ll} 7.21 + 0.0223 Q_{non-WWTP} & ext{for the 48 tributaries} \\ 10.68 & ext{for the urban headwater} \end{array}
ight.$$

where $C_{non-WWTP}$ (µg/L) is expressed as a function of $Q_{non-WWTP}$ (m³/s). The Illinois River at Henry station, as the most downstream sampling station and located near the middle of the river, was used for validation of the HAN-FP simulations. In the first scenario, only WWTPs are considered as the sources of HAN-FP. Modeling was conducted using the median as well as the first and third quartile (Q1 and Q3, See Table S5) of HAN-FP concentration in the WWTP effluents. As shown in Fig. 5a, the

simulated values using the median HAN-FP of WWTPs are well below the measured values. While the measured HAN-FP at this station on October 24 and November 22, 2019, is respectively equal to 10.82 and 11.28 $\mu g/L$, the simulated value only using the median of HAN-FP concentration in WWTP effluents is respectively equal to 4.97 and 4.07 $\mu g/L$, i.e., a mean absolute error of 6.53 $\mu g/L$ (See Text S2). Although using the third quartile (Q3) value for the HAN-FP in WWTP effluents reduces the mean absolute error to 4.79 $\mu g/L$, it is still about 43% underestimation of the measured values. In contrast, the simulation after incorporation of the estimated non-WWTP sources of HAN-FP significantly improved (Fig. 5b). The mean absolute error value is reduced to 0.55 $\mu g/L$ (Table S7).

The longitudinal profiles of HAN-FP along the river on the two selected high-flow and low-flow days (October 1 and December 20, 2019; see Section 3.1.) using the two scenarios: (i) only considering



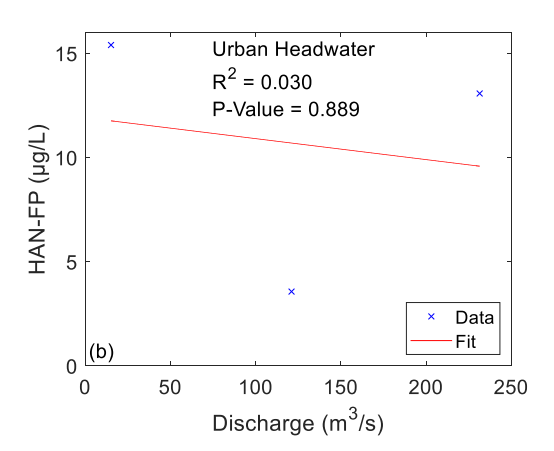


Fig. 4. Estimation of non-wastewater sources of HAN-FP in the Illinois River basin by establishing a relationship between the non-WWTP discharge and the non-wastewater-derived HAN-FP concentration: (a) Using the measurements in two tributaries (Fox River at Ottawa, IL and Kankakee River near Wilmington, IL); (b) Using the measurements of the Des Plaines River at Route 53 at Joliet, IL.

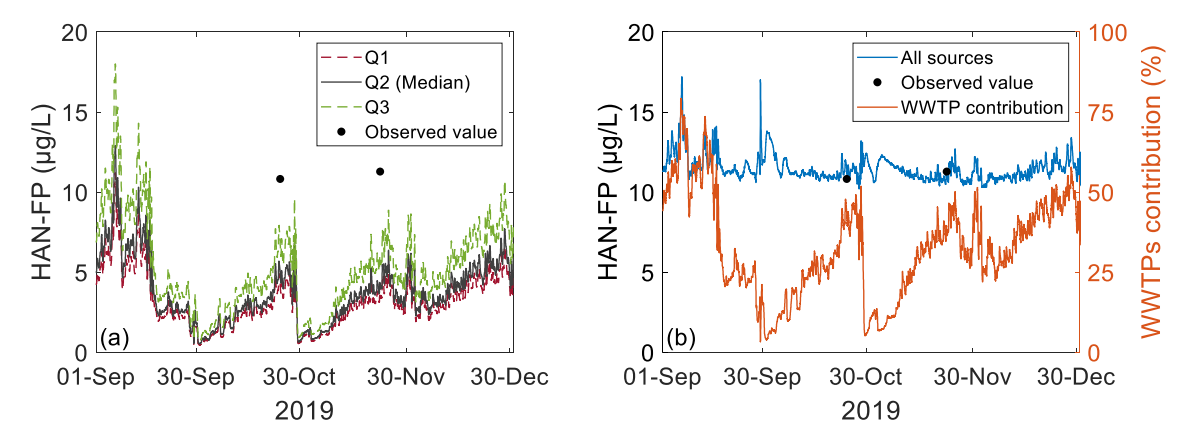


Fig. 5. The results of simulation of HAN-FP at the validation station, Illinois River at Henry, IL between September 01 and December 31, 2019. Two scenarios are used (a) the WWTPs are considered as the only sources of HAN-FP, simulations are conducted for the median (Q2) of the HAN-FP in WWTP effluents as well as the first and third quartile (Q1 and Q3), (b) the non-wastewater sources of HAN-FP are also estimated and considered in addition to the median values (Q2) of HAN-FP for WWTP effluents.

the WWTP as the sources of HAN-FP, and (ii) incorporating the estimated non-WWTP sources in addition to the WWTPs, are presented in Fig. 6. The contribution of the WWTPs in the HAN-FP along the river is also estimated by dividing the simulated HAN-FP in the first scenario by that in the second scenario. The average contribution of WWTPs to the HAN-FP along the river in the high-flow situation is 15% which is increased to 42% in a low-flow situation. Also, as can be seen in the low-flow situation that the contribution of WWTPs is generally deriving the HAN-FP concentration, the WWTPs contribution is about 100% at the urban upstream and then gradually reduces to about 24% in the downstream boundary of the model domain. This implies that even during the low-flow situation, as much as 76% of the HAN-FP export from the Illinois River to the Mississippi River, is

estimated to be originated from non-WWTP sources. While in the high flow situation, the contribution of the WWTPs is reduced to 41% in the upstream river segments and reaches values as low as about 4% in the mid-sections of the river (i.e., 96% of the HAN-FP in the mid-sections can be originated from non-WWTP sources). However, due to the complexity of the watershed with temporal dynamics in streamflow rates for each of the different tributaries, the contribution of the WWTPs exhibits a slight increase towards the downstream of the Illinois River and reaches 22% in the downstream boundary. Table 2 summarizes additional details regarding the HAN-FP simulated values and estimated average contributions of the WWTPs. From data in Table 2, the average concentration of HAN-FP along the river does not greatly vary between upstream (13.16 μ g/L) to downstream (10.94 μ g/L). The estimated

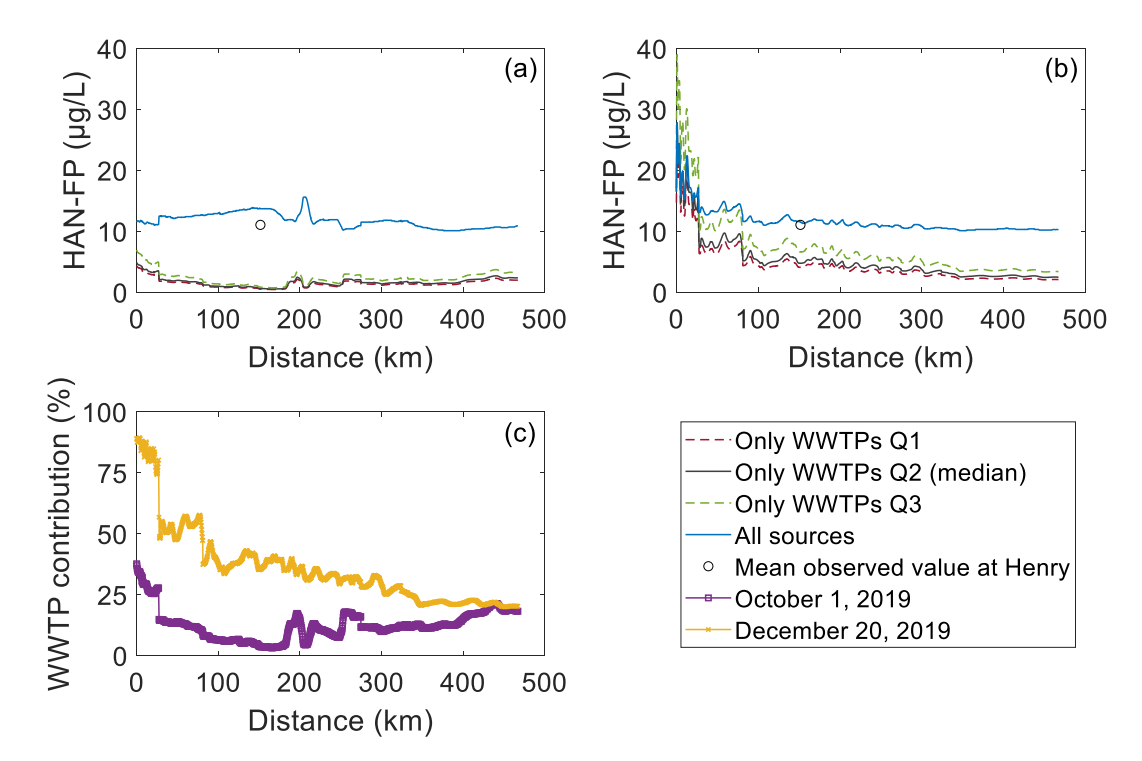
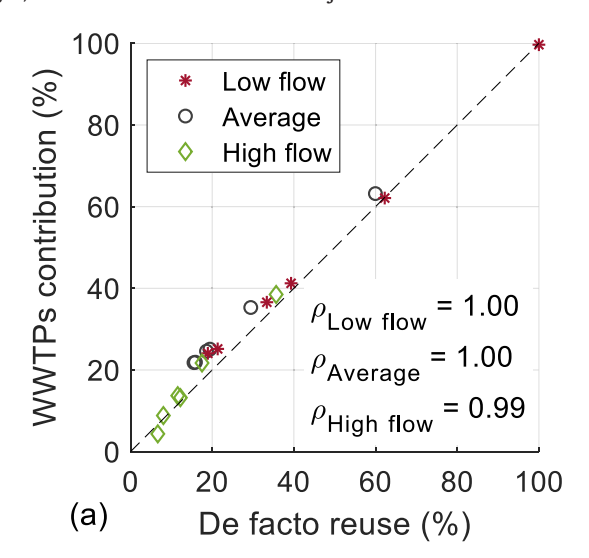


Fig. 6. The longitudinal profile of the simulated HAN-FP along the Illinois River (a) at noon October 01, 2019, which is a relatively wet and high-flow period (b) at noon December 20, 2019, which is a relatively dry and low-flow period. The mean observed HAN-FP at Henry station is just added for reference and the sampling is not done in the aforementioned days. Panel c shows the contribution of the WWTPs during high flow (October 01) and low flow (December 20) along the Illinois River. The x-axis is the distance from the most upstream location. The simulations used two scenarios: (i) considering only WWTPs as sources of HAN-FP and using the median (Q2) and the first and third quartile (Q1 and Q3) of the HAN-FP of WWTPs, and (ii) incorporating the estimated non-WWTP sources into the model in addition to the median of WWTP sources. The mean measured value of HAN-FP at the Illinois River at Henry is shown at its distance from the upstream boundary.

Table 2The HAN-FP simulation results in 6 stations along the Illinois River. The average, the standard deviation, and the minimum and maximum simulated values of the simulated HAN-FP in 4 months from September to December 2019 as well as the average contribution of the WWTPs are presented.

No.	Station name	River km	Average HAN-FP \pm STDEV (min – max) (μ g/L)	Average percentage contribution of WWTPs towards HAN-FP
1	Des Plaines River at Road 53 at Joliet, IL	1.43	13.16 ± 3.17 $(10.26-31.60)$	63%
2	Illinois River at Marseilles, IL	69.53	12.25 ± 1.28 $(10.48-21.35)$	35%
3	Illinois River at Henry, IL	150.80	11.58 ± 0.81 $(10.18-17.19)$	25%
4	Illinois River at Copperas Creek, IL	246.17	11.37 ± 0.85 $(10.05-16.72)$	25%
5	Illinois River at Meredosia, IL	351.41	11.03 ± 0.77 (9.90–15.72)	22%
6	Mississippi River at Grafton, IL	466.17	$10.94 \pm 0.75 (9.71-15.00)$	22%

average contribution of WWTPs is 63% at the upstream while it quickly decreases to below 50% in the second station and reaches the value of 22% in downstream. It shows that for the majority of the Illinois River length, the non-WWTP sources are major contributors to HAN-FP.



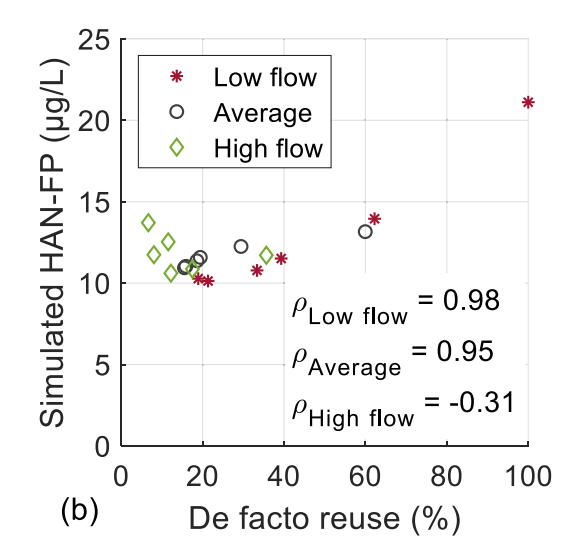


Fig. 7. Investigation of the relationship between de facto water reuse percentage and (a) the estimated contribution of WWTPs in HAN-FP, and (b) simulated HAN-FP along the Illinois River. The average calculations are considering the whole simulation period which is between September 01 and December 31, 2019. The high flow and low flow calculations are respectively corresponding to October 01 and December 20, 2019 (See Section 3.1 for the dates and Table 2 for selected stations along the river).

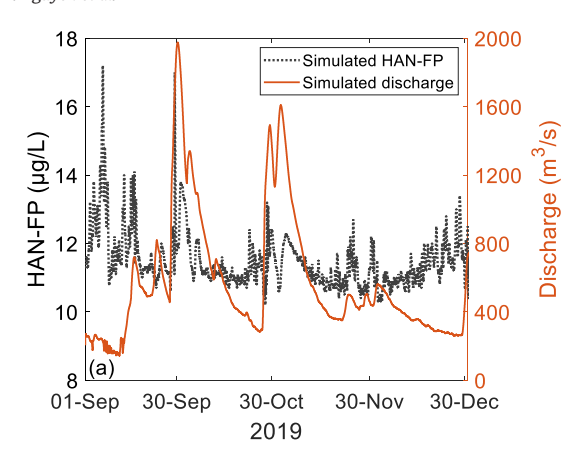
3.3. The relation between de facto reuse percentage and contribution of WWTPs in the total concentration of HAN-FP

The spatially- and temporally-resolved hydrodynamic model captures the unsteadiness of dynamic flows and permits calculation of the de facto water reuse percentage at any given time along the river. The de facto water reuse percentage has been previously used to locate the hotspots where the WWTP impact can be high in water resources (Nguyen et al., 2018). For HAN-FP, however, our results show that non-WWTP sources also contributed a significant portion of the HAN-FP in the Illinois River especially during high flow periods. The comparison of the de facto reuse percentage and the contribution of the WWTPs to the concentration of the HAN-FP as well as the comparison of the de facto reuse percentage with the simulated HAN-FP along the Illinois River are presented in Fig. 7 (See Table 2 for selected stations).

As shown in Fig. 7a, the Pearson correlation coefficients between de facto water reuse percentage and the estimated contribution of WWTPs in HAN-FP for the average, during high flow on October 1, 2019, and during low flow on December 20, 2019, are all very close to unity. This strong correlation between the two indicators shows that the de facto water reuse percentage can be used as an indicator of the contribution of the WWTPs into the HAN-FP along the river. From Fig. 7b, the relationship between de facto water reuse percentage and the HAN-FP is not always positively correlated. While there is a positive correlation between de facto water reuse percentage and the HAN-FP during the low flow situation as well as the average of the simulation period. However, the correlation coefficient during the high flow period is not significant (p-value = 0.54 imes 0.05). This observation is very important because it implies that de facto reuse percentage cannot be used as a predictor of HAN-FP concentration during high-flow periods.

3.4. The impact of flow discharge variability on HAN-FP

In contrast to the steady-flow situations previously considered (Karakurt et al., 2019), our model can examine the impact of flow variability on the HAN-FP in a complex system composed of WWTP and non-WWTP sources. As shown in Fig. 8a, while the river discharge varies considerably, ranging from below 200 m³/s to about 2000 m³/s, HAN-FP concentration is relatively stable, varying between 10.18 µg/L and 17.19 µg/L. This behavior can be attributed to the joint contribution of WWTP and non-WWTP sources to HAN-FP. Fig. 8b shows that the relationship between simulated HAN-FP and flow (Illinois River at Henry station) follows a sag curve; the highest HAN-FP concentrations are observed close to both the highest and the lowest discharges. During the low flows, the contribution of WWTP effluents in the river is high and HAN-FP concentrations can be attributed to a higher de facto reuse percentage. As streamflow discharge increases, the WWTP effluents can be diluted by the non-WWTP flow that has a lower HAN-FP concentration.



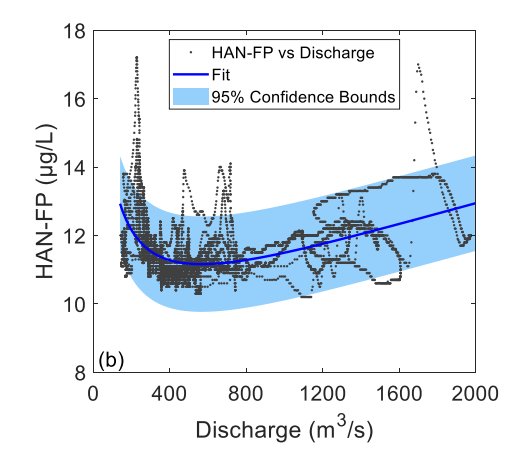


Fig. 8. The analysis of simulated streamflow discharge and HAN-FP concentration in Illinois River at Henry, IL. Panel a, shows the time series of the simulated streamflow discharge and the HAN-FP concentration. Panel b, shows the HAN-FP concentration plot against the streamflow discharge as well as the fitted Load Apportionment Model for this station.

However, as streamflow discharge further increases, so does the non-WWTP sources of HAN-FP concentration, and the total HAN-FP concentration during very high flows can become equal to or greater than that during low flows.

Using the simulated HAN-FP versus discharge data at the Henry station, the LAM model for HAN-FP is found to be as follows:

$$C_{IR} = 52.76Q_{IR}^{-0.3159} + 0.1176Q_{IR}^{0.5579} 143 < Q < 1975$$
 (8)

where C_{IR} is the HAN-FP concentration at the Henry station (µg/L) and Q_{IR} is the streamflow discharge (m³/s). The fitted function is shown in Fig. 8b and its goodness of fit parameters are $R^2 = 0.24$ and Root Mean Square Error (RMSE) = 0.71. Based on Eq. (8) the HAN-FP at both ends of the streamflow discharge range (Q = 143 or 1975 m³/s) is high, but the estimated contribution of wastewater sources is 85% when Q = 143 m³/s and decreases to 37% when Q = 1975 m³/s. Although the performance of the model is not good due to the simplifying assumption underlying the LAM model, Fig. 8b and Eq. (8) can show that there may be a persistence risk of HAN-FP pollution at all flow discharges.

3.5. Assessment of WWTP improvement scenario

Considering that nitrification is one of the most important strategies WWTPs can implement to reduce the HAN-FP of their effluents (Krasner et al., 2009; Zeng and Mitch, 2016), a management scenario analysis was performed by adding the nitrification units to the WWTPs that currently do not implement nitrification to predict the impact on HAN-FP in Illinois Rivers. The median HAN-FP of WWTPs that do not have nitrification is 28.5 μ g/L while it is equal to 13.0 μ g/L for a WWTP with a good nitrification unit. This implies that adding nitrification units to WWTPs that do not have nitrification is equivalent to a 54% reduction of HAN-FP loading from WWTP without any change in the de facto reuse percentage. The model was run assuming that all the WWTPs have good nitrification and the outcomes of this scenario along the river are presented in Table 3. Since most of the large

WWTPs near urban headwaters already have nitrification units (See Fig. 2), the expected reduction in average HAN-FP concentration is not substantial (generally below 5%). This is because the 84 WWTPs (i.e., 28% of all WWTPs) that currently practice nitrification are fairly large and account for 86% of the total WWTP effluent discharge capacity. As a result, adding a nitrification unit to the remaining 215 WWTPs will only incrementally reduce HAN-FP loading from 14% of the total flow of WWTP discharges. However, the contribution of WWTPs in the total HAN-FP will be reduced under this scenario, while the de facto reuse percentage is not supposed to change.

4. Conclusions

An integrated framework for spatiotemporal modeling of HAN-FP is developed and applied to the Illinois River basin using the HEC-RAS software. For the first time, both the WWTP and non-WWTP sources of HAN-FP are estimated and their contribution is analyzed. Considering the non-WWTP sources is critical for capturing the HAN-FP concentrations. De facto water reuse percentage can be a good predictor for the HAN-FP concentration along the river on average and during low flow events, but it is not applicable during high flow events where other watershed sources of HAN-FP dominate the precursor pool (e.g., runoff from forested watersheds). Given the significance of non-WWTP sources, adding nitrification units to the WWTPs that do not have a good nitrification process in the Illinois River basin is not an efficient solution to reduce HAN-FP concentration in the river. HAN-FP concentrations can be high both during low flows and high flows. The high concentration during low flows is due to WWTP sources, while the high concentration during high flows is owed to non-WWTP sources. This finding is important for consideration in the management of wastewater-impacted rivers. In addition, this study contributes to the formation of a paradigm for the management of nitrogenous DBPs by showing that the importance of non-WWTP sources must be recognized. In future works, using a larger database of sampling frequencies and locations, the developed framework can be expanded to study the

Table 3Results of the management scenario of adding nitrification unit to all the WWTPs that do not have a nitrification unit in the Illinois River basin.

No.	Station name	River km	Expected HAN-FP reduction (%)	Contribution of WWTPs in HAN-FP (%)	
				Before reduction	After reduction
1	Des Plaines River at Road 53 at Joliet, IL	1.43	3.9	63.2	61.7
2	Illinois River at Marseilles, IL	69.53	4.2	35.3	32.6
3	Illinois River at Henry, IL	150.8	3.3	25.1	22.6
4	Illinois River at Copperas Creek, IL	246.17	3.3	24.6	22.0
5	Illinois River at Meredosia, IL	351.41	3.0	21.9	19.3
6	Mississippi River at Grafton, IL	466.17	3.1	21.8	19.1

contribution of specific land use and land covers in delivery of HAN-FP precursors to the rivers using hydrologic watershed models.

Supplementary data to this article can be found online at https://doi.org/10.1016/j.scitotenv.2021.148355.

CRediT authorship contribution statement

Hamed Khorasani: Conceptualization, Methodology, Software, Formal analysis, Investigation, Resources, Writing – original draft, Data curation, Visualization. Jiale Xu: Conceptualization, Methodology, Software, Formal analysis, Investigation, Resources, Writing – original draft, Data curation, Visualization. Thuy Nguyen: Methodology, Software, Formal analysis, Investigation, Resources, Writing – original draft, Visualization. Zachary Kralles: Formal analysis, Investigation, Resources, Writing – review & editing. Paul Westerhoff: Conceptualization, Methodology, Resources, Writing – review & editing, Supervision, Project administration, Funding acquisition. Ning Dai: Conceptualization, Methodology, Resources, Writing – review & editing, Supervision, Project administration, Funding acquisition. Zhenduo Zhu: Conceptualization, Methodology, Resources, Writing – review & editing, Supervision, Project administration, Funding acquisition.

Declaration of competing interest

The authors declare that they have no known competing financial interests or personal relationships that could have appeared to influence the work reported in this paper.

Acknowledgment

Helps from Paul J. Terrio of the USGS Central Midwest Water Science Center in gathering the water samples from the Illinois River is kindly appreciated. This research was funded by the National Science Foundation (Grant #1805058 and #1804229).

References

- Bellrose, F.C., Mills, H.B., Starrett, W.C., 1966. Man's Effect on the Fish and Wildlife of the Illinois River, Biological Notes; no. 57. https://doi.org/10.5962/bhl.title.15157.
- Bond, T., Huang, J., Templeton, M.R., Graham, N., 2011. Occurrence and control of nitrogenous disinfection by-products in drinking water a review. Water Res. https://doi.org/10.1016/j.watres.2011.05.034.
- Borisover, M., Laor, Y., Saadi, I., Lado, M., Bukhanovsky, N., 2011. Tracing organic footprints from industrial effluent discharge in recalcitrant riverine chromophoric dissolved organic matter. Water Air Soil Pollut. 222, 255–269. https://doi.org/10.1007/s11270-011-0821-x.
- Bowes, M.J., Smith, J.T., Jarvie, H.P., Neal, C., 2008. Modelling of phosphorus inputs to rivers from diffuse and point sources. Sci. Total Environ. 395, 125–138. https://doi.org/10.1016/j.scitotenv.2008.01.054.
- Chen, B., Westerhoff, P., 2010. Predicting disinfection by-product formation potential in water. Water Res. https://doi.org/10.1016/j.watres.2010.04.009.
- Chow, A.T., O'Geen, A.T., Dahlgren, R.A., Díaz, F.J., Wong, K.-H., Wong, P.-K., 2011. Reactivity of litter leachates from California oak woodlands in the formation of disinfection by-products. J. Environ. Qual. 40, 1607–1616. https://doi.org/10.2134/jeq2010.0488.
- Chow, A.T., Díaz, F.J., Wong, K.-H., O'Geen, A.T., Dahlgren, R.A., Wong, P.-K., 2013. Photochemical and bacterial transformations of disinfection by-product precursors in water. J. Environ. Qual. 42, 1589–1595. https://doi.org/10.2134/jeq2013.01.0022.
- Darbandsari, P., Kerachian, R., Malakpour-Estalaki, S., Khorasani, H., 2020. An agent-based conflict resolution model for urban water resources management. Sustain. Cities Soc. https://doi.org/10.1016/j.scs.2020.102112.
- Diana, M., Felipe-Sotelo, M., Bond, T., 2019. Disinfection byproducts potentially responsible for the association between chlorinated drinking water and bladder cancer: a review. Water Res. https://doi.org/10.1016/j.watres.2019.07.014.
- Doederer, K., Gernjak, W., Weinberg, H.S., Farré, M.J., 2014. Factors affecting the formation of disinfection by-products during chlorination and chloramination of secondary effluent for the production of high quality recycled water. Water Res. 48, 218–228. https://doi.org/10.1016/j.watres.2013.09.034.
- Dotson, A., Westerhoff, P., Krasner, S.W., 2009. Nitrogen enriched dissolved organic matter (DOM) isolates and their affinity to form emerging disinfection by-products. Water Sci. Technol. https://doi.org/10.2166/wst.2009.333.
- Eckard, R.S., Bergamaschi, B.A., Pellerin, B.A., Kraus, T., Hernes, P.J., 2020. Trihalomethane precursors: land use hot spots, persistence during transport, and management options. Sci. Total Environ. 742, 140571. https://doi.org/10.1016/j.scitotenv. 2020.140571.

- Good, K.D., VanBriesen, J.M., 2019. Coal-fired power plant wet flue gas desulfurization bromide discharges to U.S. watersheds and their contributions to drinking water sources. Environ. Sci. Technol. 53, 213–223. https://doi.org/10.1021/acs.est.8b03036.
- Hach Company, 2015. Hach method 8155: determination of ammonia nitrogen by the salicylate method. Water Analysis Handbook, pp. 1–6.
- Iqbal, M., Taylor-Edmonds, L., Ebrahimi, S., Zollbrecht, N., Andrews, R.C., 2020. Low toxicological impact of wastewaters on drinking water sources. Water Res. https://doi.org/10.1016/j.watres.2019.115376.
- Kalin, L., Isik, S., Schoonover, J.E., Lockaby, B.G., 2010. Predicting water quality in unmonitored watersheds using artificial neural networks. J. Environ. Qual. 39, 1429–1440. https://doi.org/10.2134/jeq2009.0441.
- Karakurt, S., Schmid, L., Hübner, U., Drewes, J.E., 2019. Dynamics of wastewater effluent contributions in streams and impacts on drinking water supply via riverbank filtration in Germany - a national reconnaissance. Environ. Sci. Technol. https://doi.org/ 10.1021/acs.est.8b07216.
- Kolb, C., Good, K.D., VanBriesen, J.M., 2020. Modeling Trihalomethane increases associated with source water bromide contributed by coal-fired power plants in the Monongahela River Basin. Environ. Sci. Technol. 54, 726–734. https://doi.org/10.1021/acs. est.9b01544.
- Kozari, A., Paloglou, A., Voutsa, D., 2020. Formation potential of emerging disinfection by-products during ozonation and chlorination of sewage effluents. Sci. Total Environ. 700, 134449. https://doi.org/10.1016/j.scitotenv.2019.134449.
- Krasner, S.W., Westerhoff, P., Chen, B., Rittmann, B.E., Nam, S.N., Amy, G., 2009. Impact of wastewater treatment processes on organic carbon, organic nitrogen, and DBP precursors in effluent organic matter. Environ. Sci. Technol. https://doi.org/10.1021/ es802443t.
- Lee, M.-H., Hur, J., 2014. Photodegradation-induced changes in the characteristics of dissolved organic matter with different sources and their effects on disinfection by-product formation potential. CLEAN Soil, Air, Water 42, 552–560. https://doi.org/10.1002/clen.201200685.
- Li, W., Liu, H., Zhai, L., Yen, H., Hu, W., Lei, Q., Stewart, R.J., Guo, S., Ren, T., 2019. Evaluation of concentration-discharge dynamics and nitrogen export on anthropogenic inputs and stormflow across alternative time-scales. Ecol. Indic. 98, 879–887. https://doi. org/10.1016/j.ecolind.2018.11.057.
- Moriasi, D.N., Arnold, J.G., Van Liew, M.W., Bingner, R.L., Harmel, R.D., Veith, T.L., 2007. Model evaluation guidelines for systematic quantification of accuracy in watershed simulations. Trans. ASABE 50, 885–900. https://doi.org/10.13031/2013.23153.
- Muellner, M.G., Wagner, E.D., McCalla, K., Richardson, S.D., Woo, Y.-T., Plewa, M.J., 2007. Haloacetonitriles vs. regulated Haloacetic acids: are nitrogen-containing DBPs more toxic? Environ. Sci. Technol. 41, 645–651. https://doi.org/10.1021/es0617441.
- Nguyen, T., Westerhoff, P., Furlong, E.T., Kolpin, D.W., Batt, A.L., Mash, H.E., Schenck, K.M., Boone, J.S., Rice, J., Glassmeyer, S.T., 2018. Modeled De facto reuse and contaminants of emerging concern in drinking water source waters. J. Am. Water Works Assoc. https://doi.org/10.1002/awwa.1052.
- NRC, 2012. Water Reuse: Potential for Expanding the nation's Water Supply through Reuse of Municipal Wastewater, Water Reuse: Potential for Expanding the Nation's Water Supply through Reuse of Municipal Wastewater. https://doi.org/10.17226/13303.
- Phatthalung, W.N., Musikavong, C., 2019. Emerging disinfection by-products' formation potential in raw water, wastewater, and treated wastewater in Thailand. J. Environ. Sci. Heal. Part A 54, 745–758. https://doi.org/10.1080/10934529.2019.1592532.
- Plewa, M.J., Wagner, E.D., Richardson, S.D., 2017. TIC-Tox: a preliminary discussion on identifying the forcing agents of DBP-mediated toxicity of disinfected water. J. Environ. Sci. https://doi.org/10.1016/j.jes.2017.04.014.
- Qian-Yuan, W., Chao, L., Ye, D., Wen-Long, W., Huang, H., Hong-Ying, H., 2016. Elimination of disinfection byproduct formation potential in reclaimed water during solar light irradiation. Water Res. 95, 260–267. https://doi.org/10.1016/j.watres.2016.02.023.
- Rice, J., Westerhoff, P., 2015. Spatial and temporal variation in de facto wastewater reuse in drinking water systems across the U.S.A. Environ. Sci. Technol. https://doi.org/ 10.1021/es5048057.
- Rice, J., Westerhoff, P., 2017. High levels of endocrine pollutants in US streams during low flow due to insufficient wastewater dilution. Nat. Geosci. 10, 587–591. https://doi. org/10.1038/ngeo2984.
- Rice, J., Wutich, A., Westerhoff, P., 2013. Assessment of de facto wastewater reuse across the U.S.: trends between 1980 and 2008. Environ. Sci. Technol. https://doi.org/ 10.1021/sex402702
- Richardson, S.D., Postigo, C., 2015. Formation of DBPs: state of the science. Recent Advances in Disinfection By-Products, ACS Symposium Series. American Chemical Society, pp. 189–214 https://doi.org/10.1021/bk-2015-1190.ch011.
- Roccaro, P., Vagliasindi, F.G.A., Korshin, G.V., 2014. Relationships between trihalomethanes, haloacetic acids, and haloacetonitriles formed by the chlorination of raw, treated, and fractionated surface waters. J. Water Supply Res. Technol. - AQUA https://doi.org/10.2166/aqua.2013.043.
- Shah, A.D., Mitch, W.A., 2012. Halonitroalkanes, halonitriles, haloamides, and N-nitrosamines: a critical review of nitrogenous disinfection byproduct formation pathways. Environ. Sci. Technol. https://doi.org/10.1021/es203312s.
- Siddiqui, S., Conkle, J.L., Scarpa, J., Sadovski, A., 2020. An analysis of U.S. wastewater treatment plant effluent dilution ratio: implications for water quality and aquaculture. Sci. Total Environ. https://doi.org/10.1016/j.scitotenv.2020.137819.
- Swayne, M.D., Boone, C.H., Bauer, D., Lee, J.S., 1980. Wastewater in Receiving Waters at Water Supply Abstraction Points. United States Environmental Protection Agency.
- Thun, M.J., Linet, M.S., Cerhan, J.R., Haiman, C., Schottenfeld, D., 2017. Cancer Epidemiology and Prevention, Schottenfeld and Fraumeni Cancer Epidemiology and Prevention. Fourth edition. Oxford University Press https://doi.org/10.1093/oso/9780190238667.001.0001.

- Tsai, K.-P., Rogers, M.-F., Chow, A.T., Diaz, F., 2015. Prescribed fire alters dissolved organic matter and disinfection by-product precursor in forested watersheds – part II. A controlled field study. ACS Symposium Series, pp. 293–306 https://doi.org/10.1021/bk-2015-1190.ch016.
- USACE, 2016. HEC-RAS Hydraulic Reference Manual. US Army Corps of Engineers Hydrologic Engineering Center.
- USEPA, 2010. Comprehensive Disinfectants and Disinfection Byproducts Rules (Stage 1 and Stage 2): Quick Reference Guide. U. S. Environ. Prot. Agency.
- USEPA, 2016. Clean Watersheds Needs Survey 2012. United States Environmental Protection Agency.
- Weisman, R.J., Barber, L.B., Rapp, J.L., Ferreira, C.M., 2019. De facto reuse and disinfection by-products in drinking water systems in the Shenandoah River watershed. Environ. Sci. Water Res. Technol. https://doi.org/10.1039/c9ew00326f.
- Wu, J., Ye, J., Peng, H., Wu, M., Shi, W., Liang, Y., Liu, W., 2018. Solar photolysis of soluble microbial products as precursors of disinfection by-products in surface water. Chemosphere 201, 66–76. https://doi.org/10.1016/j.chemosphere.2018.02.185.
- Xu, J., Kralles, Z.T., Dai, N., 2019. Effects of sunlight on the trichloronitromethane formation potential of wastewater effluents: dependence on nitrite concentration. Environ. Sci. Technol. https://doi.org/10.1021/acs.est.9b00447.
- Sci. Technol. https://doi.org/10.1021/acs.est.9b00447.

 Xu, J., Kralles, Z.T., Hart, C.H., Dai, N., 2020. Effects of sunlight on the formation potential of Dichloroacetonitrile and Bromochloroacetonitrile from wastewater effluents. Environ. Sci. Technol. https://doi.org/10.1021/acs.est.9b06526.

- Yin, D., Wang, L., Zhu, Z., Clark, S.S., Cao, Y., Besek, J., Dai, N., 2021. Water quality related to Conservation Reserve Program (CRP) and cropland areas: evidence from multitemporal remote sensing. Int. J. Appl. Earth Obs. Geoinf. 96, 102272. https://doi.org/ 10.1016/j.iag.2020.102272.
- Zeng, T., Mitch, W.A., 2016. Impact of nitrification on the formation of N-nitrosamines and halogenated disinfection byproducts within distribution system storage facilities. Environ. Sci. Technol. 50, 2964–2973. https://doi.org/10.1021/acs.est.5b05668.
- Zhang, Y., Liang, X., 2019. Understanding organic nonpoint-source pollution in water-sheds via pollutant indicators, disinfection by-product precursor predictors, and composition of dissolved organic matter. J. Environ. Qual. https://doi.org/10.2134/jeq2018.06.0228.
- Zhang, R., Wang, F., Chu, W., Fang, C., Wang, H., Hou, M., Xiao, R., Ji, G., 2019. Microbial degradation of typical amino acids and its impact on the formation of trihalomethanes, haloacetonitriles and haloacetamides during chlor(am)ination. Water Res. 159, 55–64. https://doi.org/10.1016/j.watres.2019.04.032.
 Zhu, Z., Soong, D.T., Garcia, T., Behrouz, M.S., Butler, S.E., Murphy, E.A., Diana, M.J.,
- Zhu, Z., Soong, D.T., Garcia, T., Behrouz, M.S., Butler, S.E., Murphy, E.A., Diana, M.J., Duncker, J.J., Wahl, D.H., 2018. Using reverse-time egg transport analysis for predicting Asian carp spawning grounds in the Illinois River. Ecol. Model. 384, 53–62. https://doi.org/10.1016/j.ecolmodel.2018.06.003.